Process Biochemistry 129 (2023) 268–280

Contents lists available at ScienceDirect

Process Biochemistry

journal homepage: www.elsevier.com/locate/procbio

Photothermally controlled drug release of naproxen-incorporated mungbean starch/PVA biomaterials adding melanin nanoparticles

Kyeong-Jung Kim [a,1], Yeon-Hum Yun [b,1], Jae-Young Je [c,1], Do-Hyung Kim [d], Hye Suk Hwang [e,*], Soon-Do Yoon [a,*]

[a] Department of Biomolecular and Chemical Engineering, Chonnam National University, Yeosu, Jeonnam 59626, South Korea
[b] Department of Energy & Resources Engineering, Chonnam National University, Gwangju 61186, South Korea
[c] Major of Human Bioconvergence, School of Smart Healthcare, Pukyong National University, Busan 48513, South Korea
[d] Department of Aquatic Life Medicine, Pukyong National University, Busan 48513, South Korea
[e] Department of Biology, College of Life Science and Industry, Sunchon National University, Suncheon, Jeonnam 57922, South Korea

ARTICLE INFO

Keywords:
Functional mungbean starch-based biomaterials
Naproxen
Phothermal effect
Drug release mechanism

ABSTRACT

This study is aimed at preparing functional naproxen (NP)-incorporated biomaterials using mungbean starch, PVA, plasticizers, and melanin (MEL) nanoparticle. The biomaterials were characterized by FT-IR, FE-SEM and TGA. Their physical properties and antibacterial effects were also evaluated. Photothermal effects and NP release behavior were investigated using NIR laser irradiation. Results indicated that when compared to biomaterials without MEL, temperatures of MEL-added biomaterials were increased about 1.40 times when exposed to NIR laser for 30 min. NP release of NP-incorporated biomaterials at various temperatures and pH 5.5 was increased with increasing temperature. Results of NP release using artificial skin confirmed that NP was released continuously for 180 min. When NIR laser was irradiated for 30 min, NP release of MEL-added biomaterials were 3.13 times higher than that of biomaterials without MEL. NP release behavior at pH 5.5 followed a pseudo-Fickian mechanism, whereas it followed a non-Fickian mechanism in artificial skin.

1. Introduction

Biodegradable natural polymers-based materials have gained great attentions in the biomedical applications field as materials for fabrication of various devices [1–3]. Many studies have focused on replacing biocompatible polymers used for biomedical devices with biodegradable biomaterials using polysaccharides such as starch, glycogen, cellulose, and chitosan because of their biodegradability, biocompatibility, and affordability [4,5]. Starch consists of linear amylose and branched amylopectin, and it is mainly present in plants such as potatoes, corn, wheat, rice, cassava, mungbean, and tapioca. Owing to its advantages of biocompatibility, biodegradability, non-toxicity, and affordability, it has been applied a biomaterial in various fields including drug delivery systems, tissue engineering scaffolds, wound dressings, and bone replacement/fixation [6,7].

The delivery of drugs and bioactive substances through the skin is an attractive alternative that can minimize the side effect of oral administration. These methods are called transdermal drug delivery systems (TDDS) [8]. When compared to oral drug delivery, TDDS has the advantages of avoiding first-pass metabolism, increasing drug bioavailability, and reducing side effects without gastrointestinal disorders. However, owing to the protective action of the stratum corneum present on the skin, the ability of low molecular weight (<500 Da) and lipophilic drugs to penetrate percutaneously by passive diffusion is restricted [9].

Functional biomaterials for TDDS used in this study were prepared using mungbean starch (MS) as the main component. Mungbean, which is a native plant of Southeast Asia, is widely grown not only in the U.S.A. but also Africa, South America, and Australia. The seeds with abundant protein (about 28%) contained a high amount of starch including high amylose content (30–45%) [10]. Our previous study corroborated the characterization and drug release properties of starch-based biomaterials used in TDDS [11,12]. Additionally, there have been reports on the development of functional allopurinol mungbean starch-based

* Corresponding authors.
E-mail addresses: kimkj124@nate.com (K.-J. Kim), yhhumm@jnu.ac.kr (Y.-H. Yun), jjy1915@pknu.ac.kr (J.-Y. Je), dhkim@pknu.ac.kr (D.-H. Kim), hshwang33@scnu.ac.kr (H.S. Hwang), yunsd03@jnu.ac.kr (S.-D. Yoon).
[1] These authors contributed equally to this work.

https://doi.org/10.1016/j.procbio.2023.03.034
Received 17 January 2023; Received in revised form 27 March 2023; Accepted 30 March 2023
Available online 31 March 2023

biomaterials and their various properties, which comprise poloxamer as a temperature-sensitive polymer. The results indicated that poloxamer can increase the efficiency of drug release in functional biomaterials, demonstrating that stimulus-responsive substances in TDDS could improve skin permeability [13].

Numerous studies have used functional biomaterials that respond to various stimuli, such as pH, light, and temperature, to overcome the limitations of TDDS and improve the skin permeability of drugs [14–17]. Functional stimulus-responsive materials such as melanin (MEL), proxamer, poly(N-isopropylacrylamid), and black phosphorus are attracting attention in biomedical materials for various diseases treatment [18,19]. Of these functional stimulus-responsive materials, black phosphorus has excellent biodegradability, photothermal effect, and high specific surface area, and is a new drug delivery material for cancer treatment. However, black phosphorus is highly reactive to oxygen and water, resulting in degradation under ambient conditions. To improve the stability of black phosphorus, surface modification, and covalent functionalization methods were investigated. The problem with these methods is that they cause increased toxicity and decreased photothermal effect [20–23]. In addition, among photothermal agents, melanin (MEL), a natural polyphenol produced by melanogenesis from melanocytes, is found in both the skin and hair. MEL has the advantages of biocompatibility, UV shielding, antioxidation, and non-toxicity. It can effectively absorb light with wide wavelengths, from ultraviolet to near infrared (NIR), and convert that energy into heat. Therefore, the photothermal effect of MEL has been widely applied in photothermal therapy [24–26]. Heat can be applied locally to the skin to increase drug permeability while improving vascular perfusion [27,28]. In this study, we evaluated the control of drug release using the naproxen (NP) as an anti-inflammatory agent and investigated the enhancement of skin permeability of NP using the photothermal effect of functional biomaterials with the addition of MEL.

Inflammation, the reaction of the immune system to infections and injuries, is a series of biological mechanisms the body uses to inhibit harmful substances that have invaded tissues. The four main signs of an inflammatory response are rubor (redness), calor (heat), tumor (swelling), and dolor (pain). The general inflammatory response is characterized by a temporally restricted upregulation of inflammatory activity that occurs only in the presence of a threat. As the stimuli brought on by harmful substances are removed via phagocytosis, the inflammatory response gradually diminishes. During inflammation resolving, granulocytes are removed, and macrophages and lymphocytes return to normal pre-inflammatory levels and phenotypes [29–31]. However, when inflammation becomes uncontrolled and enters the acute phase, inflammatory macrophages increase rapidly, resulting in tissue or organ damage. Therefore, if this acute inflammation is not resolved, it can cause autoimmunity, chronic dysplastic inflammation, and cancer [32,33].

NP is one of the nonsteroidal anti-inflammatory medications used to treat a wide range of inflammation, fever, and pain. It is also used to treat diseases such as osteoarthritis, rheumatoid arthritis, gout, menstrual cramps, and migraine [34,35]. The primary mechanism of NP action is to reversibly and competitively inhibit cyclooxygenase-1 (COX-1) and cyclooxygenase-2 (COX-2), thereby preventing the conversion of arachidonic acid to the pro-inflammatory prostaglandins (PG). PG synthesis Inhibition is important in the regulation of inflammation because PG biosynthesis is significantly increased in inflammatory tissues and contributes to acute inflammation [32,36]. Although NP is highly effective, the oral formulation has side effects such as nausea, heartburn, acid dyspepsia, gastrointestinal bleeding, and gastric ulcer [37,38]. Therefore, the development of a drug delivery platform that maintains medicinal efficacy while minimizing these side effects is required.

In this study, we prepared functional NP-incorporated MS-based biomaterials using PVA, plasticizer (glycerol (GL), and L-arginine (AG)) for treating inflammation. We also investigated the NP release properties of the prepared biomaterials. In addition, MEL was used as a photothermal agent for the treatment of acute inflammation by enhancing drug release efficiency. The photothermal conversion effect and NP release properties of the prepared functional biomaterials with/without the addition of MEL were evaluated using NIR laser irradiation. The NP release mechanism was determined using well-known diffusion models (Fickian and non-Fickian diffusion models). To verify the applicability of TDDS, the release properties of the prepared functional biomaterials were also confirmed using an artificial skin test.

2. Materials and methods

2.1. Materials

Naproxen (NP), polyvinyl alcohol (PVA, 99% hydrolyzed; number average molecular weight = 89,000–98,000), glycerol (GL), L-arginine (AG), and melanin (MEL) as a photothermal agent were purchased from Sigma-Aldrich Chemical Company, Inc. (St. Louis, MO, USA). Mungbean starch (MS) was obtained from Chungwon food, Inc. (Incheon, South Korea). Distilled water (DW) was redistilled after deionization and used in all experiments.

2.2. Preparation of functional NP-incorporated mungbean starch-based biomaterials

Functional NP-incorporated MS-based biomaterials were prepared using the casting method and UV curing process. First, MS and plasticizers (GL and AG) were mixed in DW for 30 min. The PVA solution was prepared by dissolving PVA in hot DW (95 °C). Subsequently, both solutions were mixed and maintained at 95 °C for 15 min. Using a mechanical stirrer (400 rpm) the mixture was blended for 60 min at room temperature to prepare a homogeneous gel-like solution. The imprinting of NP and/or incorporation of MEL progressed during the blending process. After dissolving NP and/or MEL in DW, these solutions were added dropwise for uniform recognition and dispersion into the gel-like solution. The chemical compositions of the functional starch-based biomaterials are shown in Table 1. An aspirator was used to remove bubbles from the homogeneous gel-like solution before it was poured onto a preheated Teflon mold (40.0 °C; 250 × 250 × 1 mm). The mold was dried using a ventilated oven at 40.0 °C for 24 h. These prepared MS-based biomaterials were cured for 10, 20, 30, 40, 50, and 60 min under an atmospheric pressure UV lamp (OSRAM ULTRA-VITALUX, 300 W).

2.3. Water resistance properties

The swelling behavior (SB) and solubility (S) were measured to evaluate the water resistance properties of the starch-based biomaterials. The prepared biomaterials were immersed in DW at 25.0 °C. The surface moisture of biomaterials was removed after 24 h, when equilibrium had been attained, and the weight of each biomaterial was measured. The SB of each biomaterial was computed using the following equation (Eq. (1)):

Table 1
Component of functional NP-incorporated starch-based biomaterials.

Sample name	MS (g)	PVA (g)	AG (% wt)	GL (% wt)	NP (g)	MEL (mg)	DW (g)
MSP	5.0	5.0	-	-	-	-	100
MSPNP	5.0	5.0	-	-	0.5	-	120
MSPAGNP	5.0	5.0	40	-	0.5	-	120
MSPGLNP	5.0	5.0	-	40	0.5	-	120
MSPMELNP	5.0	5.0	-	-	0.5	5	120
MSPAGMELNP	5.0	5.0	40	-	0.5	5	120
MSPGLMELNP	5.0	5.0	-	40	0.5	5	120

$$\text{Swelling behavior(SB)} = \frac{(W_e - W_0)}{W_0} \quad (1)$$

where W_e is the weight of the swelling biomaterial at equilibrium, and W_0 is the initial weight of the dried biomaterial.

The swollen biomaterials were dried again at 50.0 °C for 24 h. The S value of each biomaterial was computed using the following equation (Eq. (2)):

$$\text{Solubility(S)} = \frac{(W_0 - W_d)}{W_d} \quad (2)$$

where W_0 is the initial weight of the dried biomaterial and W_d is the dry weight of the swollen biomaterial.

2.4. Mechanical properties

The tensile strength (TS) and elongation at break (%E) of the prepared starch-based biomaterials were investigated using the Instron 6012 testing machine (Norwood, MA, USA). Six dumbbell-shaped specimens (ASTM D-412) were cut out of the prepared biomaterials. The thickness of the prepared biomaterials was measured thrice using a mechanical scanner (Digital thickness gauge "Mitutoyo" Tokyo, Japan) around the biomaterials, and their average thickness was 0.122 ± 0.004 mm. The gauge length and grip distance were both 53.0 mm. The crosshead speed was set at 20 mm/min, and the load cell capacity was 250 kg_f. All tests were performed at 25 °C with 58.0% RH.

2.5. Characterization

The surface and cross-section of the prepared MS-based biomaterials with/without NP, MEL, and plasticizers were analyzed by field emission scanning electron microscopy (FE-SEM, ZEISS Sigma 500, Carl Zeiss Co., Ltd, Germany) at an acceleration voltage of 5.0 kV. Fourier transform infrared spectrophotometry (FT-IR) analysis of NP, MEL, and prepared biomaterials was performed using an FT-IR spectrophotometer (vertex-70, Bruker, Germany).

2.6. Evaluation of antimicrobial activities

To determine antimicrobial activities of biomaterials, 2 types of Gram-positive bacteria (*Staphylocccus aureus* ATCC29213 and *Staphylocccus epidermidis* TMPSB-D10) and 3 types of Gram-negative bacteria (*Escherichia coli* ATCC25922, *Edwardsiella tarda* ATCC15947, and *Salmonella enterica* ATCC7001) were used. Nutrient broth was used to grow bacteria at 37 °C. The antibacterial effect of the biomaterials was determined using an agar plate method. A bacterial suspension (10^7 – 10^6 CFU/mL) was evenly spread on the Tryptic Soy Agar plates, followed by placing sterilized the biomaterials. The plates were then incubated at 37 °C for 18–36 h. The antibacterial effect of the films was assessed by checking the growth of bacteria under the biomaterials.

2.7. Photothermal conversion effects

To evaluate the photothermal conversion effect of the functional starch-based biomaterials with MEL, the prepared biomaterials were irradiated with an 808 nm NIR laser (LAB808CW-4 W-f400, Laserlab Co., Seoul, Korea) at a power density of 1.5 W/cm^2 for 30 min [39]. The temperature variations of the prepared biomaterials were observed every 10 min using an infrared thermal camera (C2, FLIR System Inc., Sweden).

2.8. Thermogravimetric measurements

Thermogravimetric measurements for prepared biomaterials were performed using a DSC Q200/TGA Q50 (TA Instruments, USA) from 25° to 600°C in a N_2 environment (flow rate, 20 mL/min) at a heating rate of 10 °C/min. The sample weight was between 10.0 and 11.0 mg.

2.9. NP release properties

The NP release from the functional NP-incorporated starch-based biomaterials was estimated under various temperatures (32.0 °C for cold skin temperature, 36.5 °C for natural skin temperature, and 40.0 °C for inflammatory temperature) and pH 5.5 buffer solution as a human skin condition [40,41]. The NP-incorporated biomaterials (0.10 g) were immersed in flasks containing 30 mL buffer solution. These flasks were incubated in a shaking incubator (VS-8480SF, Vision, Scientific Co., Korea) at 50 rpm and 32.0, 36.5, or 40.0 °C. The release medium was collected at a predetermined time and released NP was measured using a UV–vis spectrophotometer (OPTIZEM 2120UV, Neogen, Co., Ltd, Korea) at 329 nm. These cumulative concentrations (%) of released NP were calculated using a standard calibration curve. The possibility of using the prepared biomaterials as TDDS was also verified via a drug release test using artificial skin (Neoderm-ED, Tego science, Inc. Korea). The prepared NP-incorporated biomaterials (2.0 × 2.0 cm) were placed on artificial skin mixed with agar-based gel at 36.5 °C and RH 60.0%. Thereafter, agar-based gel was then immersed in DW at 25 °C for 8 h. The NP release was quantified using a UV–vis spectrophotometer. Furthermore, based on the specific photothermal effect of MEL, the improvement of drug release efficiency of the functional NP-incorporated MS-based biomaterials as a result of MEL addition was confirmed using 808 NIR laser irradiation. The prepared biomaterials were investigated via an artificial skin test (36.5 °C and RH 60.0%.) with/without 808 nm NIR laser irradiation at a power density of 1.5 W/cm^2 for 30 min

To verify the drug delivery mechanism, Fickian diffusion and empirical models were calculated. Fick's law can be used to estimate the diffusion coefficient of a targeted drug in a macromolecular system (Eq. (3)) [42,43].

$$\frac{\partial C}{\partial t} = D\frac{\partial^2 C}{\partial x^2} \quad (3)$$

where C is the diffusion molecule concentration at time t and D is the constant diffusion coefficient.

In the thin polymer slab, the solution of Eq. (3) is rearranged in the form of a trigonometric series and can be expressed as follows: where, if diffusion of a drug in the x direction occurs in a polymer slab of thickness l ($-\frac{l}{2} < x < \frac{l}{2}$), the appropriate boundary conditions are

$$c(t=0,x);\ \frac{\partial c}{\partial t}(t, x=0);\ C\left(t, x=\frac{l}{2}\right) = C_{eq} \quad (4)$$

In Eq. (4), C_{eq} is the final equilibrium concentration of drug diffusion. Using these conditions in the thin polymer slab, Eq. (3) is rearranged in the form of a trigonometric series, and can be expressed as Eq. (5).

$$\frac{C(t,x)}{C_{eq}} = 1 - \frac{4}{\pi}\sum_{n=0}^{\infty}\frac{(-1)^n}{2n+1}\exp\left(\frac{-D(2n+1)^2\pi^2 t}{l^2}\right)\cos\left(\frac{(2n+1)\pi x}{l}\right) \quad (5)$$

Integrating Eq. (5) is expressed as Eq. (6), which is known as the Fickian diffusion model [44,45].

$$\frac{Q_t}{Q_\infty} = 1 - \sum_{n=0}^{\infty}\frac{8}{(2n+1)^2 \bullet \pi^2}\exp\left[-\frac{D_e \bullet (2n+1)^2\pi^2}{l^2} \bullet t\right] \quad (6)$$

where Q_t is the amount of drug released at time t, $Q_\infty$is the amount of drug released at infinite time, l is the half thickness of the slab, and t is the diffusion time, and D_e is diffusion coefficient.

The empirical model is also expressed as follows (Eq. (5)) [46,47]:

$$\frac{Q_t}{Q_\infty} = kt^n \quad (7)$$

where k is the drug release constant and n is the diffusional exponent, indicative of the mechanism of drug release. In the case of $n < 0.5$, the release behavior indicates a pseudo-Fickian diffusion mechanism. A value of $n = 0.5$ implies a Fickian diffusion mechanism, and values of n between 0.5 and 1.0 are related to a non-Fickian diffusion mechanism [48,49].

2.10. Statistical analysis

All experiments were performed in triplicate (n = 3). The test results are expressed as mean ± standard deviation (SD). The experimental results of this study were evaluated for statistical significance via t-test ($p < 0.05$) with repeated experiments.

3. Results and discussion

3.1. Physical properties of functional MS-based biomaterials

Evaluation of swelling behavior (SB) and solubility (S) is crucial for confirming the water resistance of biomaterials and the degree of crosslinking between their components. To ascertain the optimal UV curing conditions for the MS-based biomaterials, the SB and S of the prepared biomaterials were evaluated with various UV curing times. Fig. 1a and b show the results of SB and S of the MS-based biomaterials with/without the addition of plasticizers (AG and GL) prepared by UV curing. The SB and S values of the prepared biomaterials decreased as the UV curing time increased. These results imply that the water resistance and the degree of crosslinking of the prepared biomaterials by UV curing were improved. However, when UV curing time was more than 30 min, the SB and S values did not change significantly. Therefore, the functional MS-based biomaterials were prepared by setting the optimal UV curing condition to 30 min. Biomaterials with AG and GL had a decrease in SB, whereas the biomaterials with only GL had the lowest SB values and the highest S values. These results indicate that the binding strength was relatively weak because there were few functional groups capable of hydrogen bonding in the GL-added biomaterials among the prepared biomaterials.

The mechanical properties of starch-based biomaterials are important factors for applications in various biomedical engineering fields. The results of TS and %E for the prepared biomaterials with/without the addition of NP, MEL, and plasticizers (AG and GL), in which the UV curing process was performed for 30 min, are shown in Fig. 1. c and d. The results reveal that the TS and E% of the biomaterials with MEL were not significantly different from those of biomaterials without MEL. When AG or GL was added to the MS-based biomaterials, the TS values were lower than those of biomaterials without of AG or GL, whereas the %E values of biomaterials without the AG or GL were higher than those of the biomaterials without AG or GL. However, the addition of NP did not significantly affect the mechanical properties of the prepared biomaterials.

3.2. Characterization

To verify the stability of NP and the functional prepared NP-incorporated MS-based biomaterials via UV irradiation, UV irradiated NP and biomaterials were analyzed by FT-IR. The results of the FT-IR

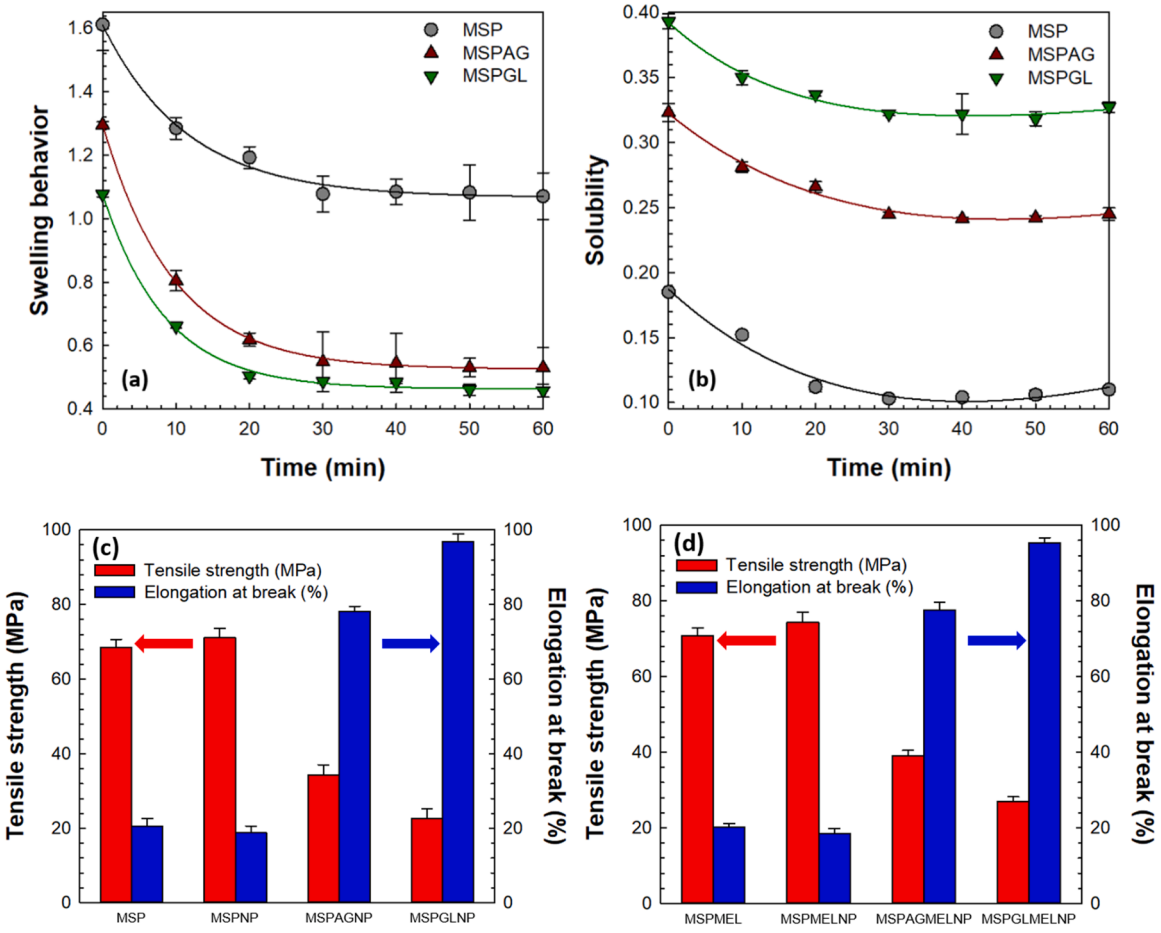

Fig. 1. Physical properties of starch-based biomaterials with UV curing. (a) Swelling behavior of starch based biomaterials with various UV curing time. (b) Solubility of starch based biomaterials with various UV curing time. (c) Tensile strength (TS) and elongation at break (%E) of starch based biomaterials with/without the addition of NP and plasticizers. (d) TS and %E of starch based biomaterials with/without the addition of NP, MEL and plasticizers.

analysis for the stability of NP before and after UV curing are shown in Fig. 2a. A sharp peak at 1585 cm^{-1} corresponded to COO^-, which is a characteristic functional group peak of NP, and peaks at 3059 and 2910 cm^{-1} corresponded to aromatic C-H and aliphatic C-H stretching, respectively [50,51]. In the FT-IR spectra of MEL (see Fig. 2b), a broad absorption band at 3224 cm^{-1} for OH stretching, a peak at 1704 cm^{-1} due to carbonyl group vibration, and a strong peak at 1609 cm^{-1} related to aromatic ring C═C were confirmed [52,53]. Therefore, the FT-IR spectra of NP and MEL revealed that UV curing did not deform their structures under the preparation condition of functional biomaterials. Fig. 2c shows the FT-IR spectra of the prepared biomaterials with/-without the addition of NP. Peaks at 849, 925, and 1146 cm^{-1} were associated with the -C-O-C- ring vibration of granular starch, and the strong peak at 1018 cm^{-1} corresponded to the characteristic peak of anhydrous starch ring O-C stretch. Absorption bands at 1329 and 1414 cm^{-1} due to bending vibration of -CH in -CH_2OH were observed [54]. The biomaterials with AG peaked around near 1632 cm^{-1}, which is a characteristic peak for the guanidine group of AG [55]. The broad absorption bands of 2921 and 3275 cm^{-1} in the biomaterials with GL were attributed to the hydroxyl group of GL. Results of FT-IR analysis of the NP-incorporated biomaterials indicated that the specific peaks of NP appeared at 1563–1592 cm^{-1}. However, characteristic peaks of MEL were not verified because of overlapping, similarities of chemical structures, and the small amount of MEL.

Fig. 3 shows the results of FE-SEM images for the surface and cross-section analysis of the prepared functional biomaterials. The prepared biomaterials were generally uniform without noticeable porosity, crack, or flaw. Furthermore, the biomaterial surface and cross-sectional characteristics were not influenced by the UV curing process. Fig. 3(e – h) show that the MEL-added biomaterials have a darker color than those of biomaterials without the addition of MEL because MEL has a black or brown color.

3.3. Antimicrobial activities

The antibacterial effect of the biomaterials was evaluated, and the results are shown in Fig. 4 and Table 2. From the results, it could be found that no antibacterial effect for Gram-negative bacteria of the biomaterials was observed. Whereas, the biomaterials showed the antibacterial effect against *S. aureus* and *S. epidermidis*. Among them, MSPGLNP and MSPGLMELNP weakly inhibited the growth of *S. aureus* with the concentration of 10^6 and 10^7 CFU/mL. In addition, MSPGLNP, MSPGLMELNP, and MSPAGMELNP films also showed the growth inhibitory effect for *S. epidermidis* with the concentration of 10^6 and 10^7

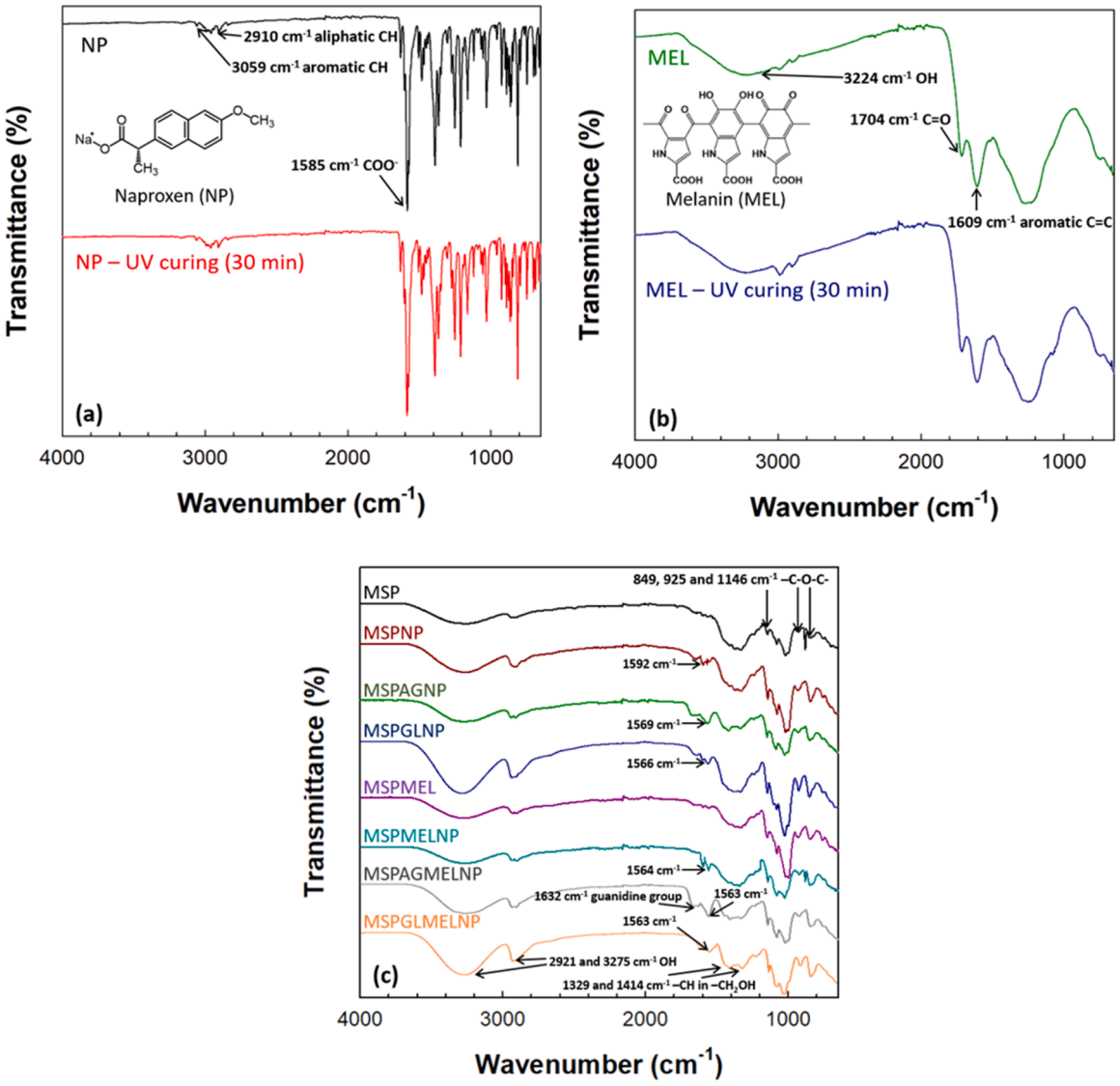

Fig. 2. FT-IR spectra of NP, MEL and functional NP-incorporated biomaterials. (a) FT-IR spectra of NP with/without UV curing. (b) FT-IR spectra of MEL with/without UV curing. (c) NP-incorporated biomaterials with/without the addition of NP, MEL, and plasticizers.

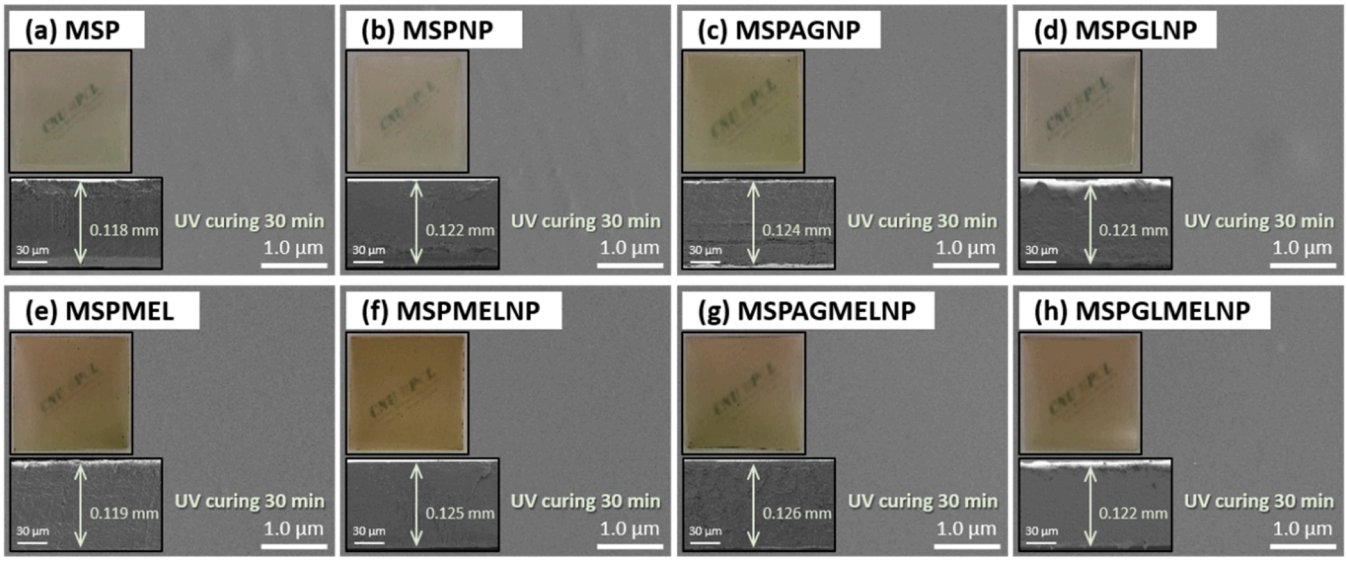

Fig. 3. FE-SEM images of surfaces and cross-sections of functional biomaterials. (a) starch-based biomaterials without the addition of NP, MEL, and plasticizers. (b) NP-incorporated starch-based biomaterials. (c) AG-added NP-incorporated starch-based biomaterials. (d) GL-added NP-incorporated starch-based biomaterials. (e) MEL-added starch-based biomaterials without the addition of NP and plasticizers. (f) MEL-added NP-incorporated starch-based biomaterials. (g) MEL-added NP-incorporated starch-based biomaterials with the addition of AG. (h) MEL-added NP-incorporated starch-based biomaterials with the addition of GL.

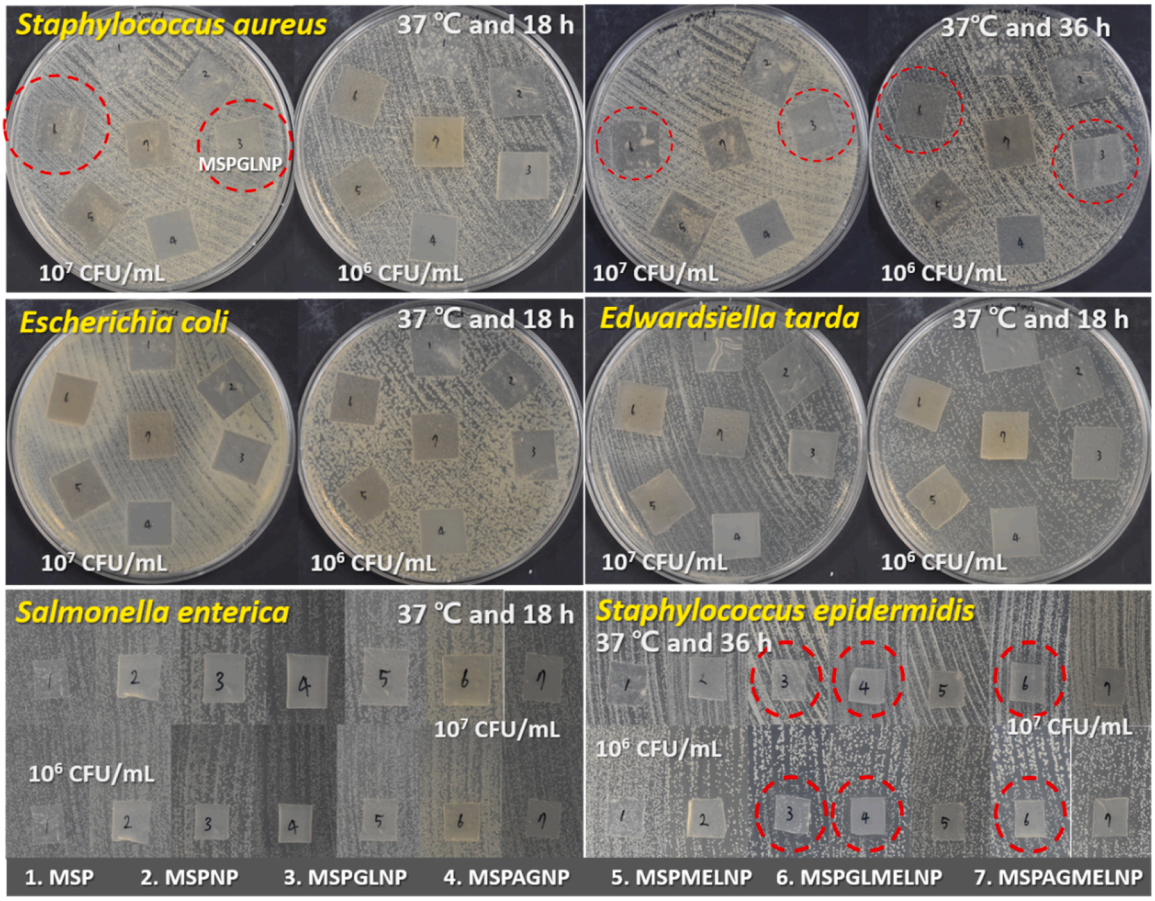

Fig. 4. Antimicrobial activities of the prepared biomaterials.

CFU/mL. Results indicated that there were no significant antibacterial activities for all biomaterials. However, it can be confirmed the stability of the prepared biomaterials against Gram-positive and Gram-negative bacteria.

3.4. Photothermal conversion effects

MEL has a harmless and excellent photothermal conversion effect. To determine whether the MEL, which was introduced as a photothermal

Table 2
Antibacterial effect of functional NP-incorporated starch-based biomaterials against some pathogenic bacteria.

Sample	*S. epidermidis*	*S. aureus*			*E. coli*	*E. tarda*	*S. enterica*
	36 h* 10^{6-7} CFU/mL	18 h 10^{6} CFU/mL	18 h 10^{7} CFU/mL	36 h 10^{6-7} CFU/mL	18 h 10^{6-7} CFU/mL	36 h 10^{6-7} CFU/mL	36 h 10^{6-7} CFU/mL
MSP	-	-	-	-	-	-	-
MSPNP	-	-	-	-	-	-	-
MSPGLNP	+	-	+	+	-	-	-
MSPAGNP	+	-	-	-	-	-	-
MSPMELNP	-	-	-	-	-	-	-
MSPGLMELNP	+	-	+	+	-	-	-
MSPAGMELNP	-	-	-	-	-	-	-

(+) susceptibility (weak inhibitory activity)
(-) absence of susceptibility
* Antibacterial assay condition

agent, increased heating efficiency, we irradiated the prepared biomaterials with a NIR laser for 30 min. As shown in Fig. 5, it could be verified that the temperature of MEL particles increased drastically to about 60.0 °C within 30 min after NIR laser irradiation. In addition, the temperature of MEL added-biomaterials without the addition of NP and plasticizers and MEL-added biomaterials with NP increased rapidly and reached about 39.0 °C within 30 min. However, the biomaterials without MEL increased only by about 3.4 °C. In the case of the biomaterials with AG/GL and MEL, the temperature increased more rapidly, and the biomaterials reached 40.5 and 41.1 °C, respectively, within 30 min. The temperature of the biomaterials with AG/GL was higher than that of the biomaterials without plasticizers because the functional groups of AG and GL could provide higher photothermal conversion efficiency by generating intermolecular interactions and creating a large free volume inside the biomaterials [56,57]. The increase in skin temperature due to heating can enhance permeability and blood flow of the skin, and heating to 42.0 – 43.0 °C does not cause pain or damage to the skin [58,59]. Therefore, these results demonstrated that the prepared functional biomaterials with MEL have a photothermal conversion effect and suggested that the drug release of the biomaterials can be improved in TDDS.

3.5. Thermogravimetric analtysis

Fig. 6 shows the results of thermogravimetric analysis (TGA) of prepared biomaterials. Three phases of weight loss were confirmed for the prepared biomaterials. The first weight loss (25–224 °C) is related to the evaporation of adsorbed and bound water molecules to the biomaterials. The second weight loss associated with the thermal decomposition of the compounds in the biomaterials occurred in the range of 224–322 °C. The weight loss continued with the temperature increased up to 550 °C. In addition, biomaterials with the addition of NP was lowered the degradation temperature in the first phase because the thermal decomposition of NP begins at 200 °C. The MEL-added biomaterials slightly reduced the weight loss in the third phase. These results are because MEL could improve the thermal stability of biomaterials [60,61]. Since plasticizers are particularly sensitive to thermal degradation, the weight loss of AG- or GL-added biomaterials was higher than that of biomaterials without the addition of plasticizers [62].

3.6. NP release properties

Fig. 7 shows the results of NP release ratio (%) from functional NP-incorporated biomaterials with/without MEL, plasticizers (AG and GL), and NIR laser irradiation at various temperatures (32.0, 36.5, and 40.0 °C) in pH 5.5 buffer solution. Figs. 7a, 7b, and 7c show the NP release ratio (%) of the NP-incorporated biomaterials with/without plasticizers and without NIR laser irradiation. Results indicated that NP was rapidly released until 15 min and then reached equilibrium within 30 min. In addition, the degree of NP releases increased as the temperature increased from 32.0 °C to 40.0 °C. Results of NP release of the prepared NP-incorporated biomaterials were obtained based on the type of plasticizer added to biomaterials in the following order: MSPGLNP > MSPAGNP > MSPNP. These results are related to the weak interaction between the biomaterials components and NP due to the lower physical properties of biomaterials with GL than other prepared biomaterials.

Figs. 7d, 7e, and 7f show the NP release ratio (%) for NP-incorporated biomaterials with MEL, with/without the addition of AG and GL, and with NIR laser irradiation. Results indicated that the NP release was increased by about 1.2 – 1.3 times with NIR laser irradiation because of the photothermal conversion effect. Additionally, the degree of NP release at 40.0 °C was found to be lower than those at 32.0 °C and 36.5 °C. This is could be because the maximum increase in temperature by NIR laser irradiation for 30 min is about 38.5 – 41.0 °C (see Fig. 5b).

Understanding the drug release mechanisms in drug-incorporated biomaterials and mathematically modeling experimental data are crucial for their potential applications as TDDS. Thus, we investigated the NP release mechanism using Fickian diffusion and empirical models to systematically elucidate the NP release behavior of the functional NP-incorporated biomaterials.

Fig. 7 and Table 3 show the comparison results after the mathematical modeling (Fickian diffusion and empirical model) of the NP release behavior of the prepared NP-incorporated biomaterials with/without plasticizers (AG and GL), MEL, and NIR laser irradiation at various temperatures in pH 5.5 buffer solution.

Figs. 7a, 7b, and 7c (long dash line and solid line) show the Fickian diffusion and empirical modeling results for the verification of NP release behavior from the AG and GL-added NP-incorporated biomaterials without MEL and NIR laser irradiation. Results indicated that the NP release behavior using the Fickian diffusion model was more suitable than those using the empirical model. In addition, the diffusion coefficient (D_e) values increased with increasing temperature (see Table 3). The D_e values of NP-incorporated biomaterials with AG and GL were higher than those of the NP-incorporated biomaterials without plasticizers. The D_e of the NP-incorporated biomaterials with GL had the highest values at various temperatures. Additionally, the result of the Fickian diffusion (long dash line) and empirical modeling (solid line) for the verification of NP release behavior from AG and GL-added NP-incorporated biomaterials with MEL and NIR laser irradiation are shown in Figs. 7d, 7e, and 7f. When compared to the calculation results of the Fickian diffusion and empirical model, the same trends were observed in previous results. In addition, it could be confirmed that the D_e values of NP release rates for the prepared NP-incorporated biomaterials with MEL were 1.10 – 1.25 times higher than those of the prepared NP-incorporated biomaterials without MEL. The empirical modeling results show that the diffusional exponents (n) of the prepared NP-incorporated biomaterials were less than 0.5. These results revealed that NP release behavior followed a pseudo-Fickian diffusion mechanism.

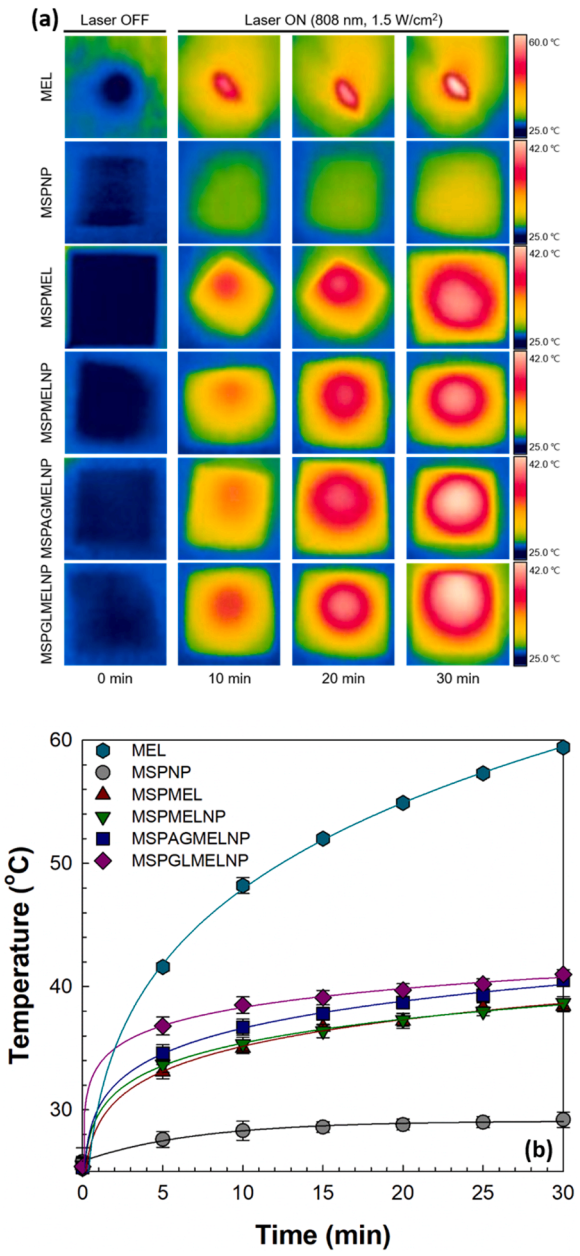

Fig. 5. Photothermal conversion effect of functional NP-incorporated biomaterials. (a) Thermal images of NP-incorporated biomaterials with/without the addition of MEL or plasticizers under 808 nm NIR laser irradiation (1.5 W/cm^2, 30 min). (b) Photothermal heating curves of NP-incorporated biomaterials with/without the addition of MEL or plasticizers under 808 nm NIR laser irradiation (1.5 W/cm^2, 30 min).

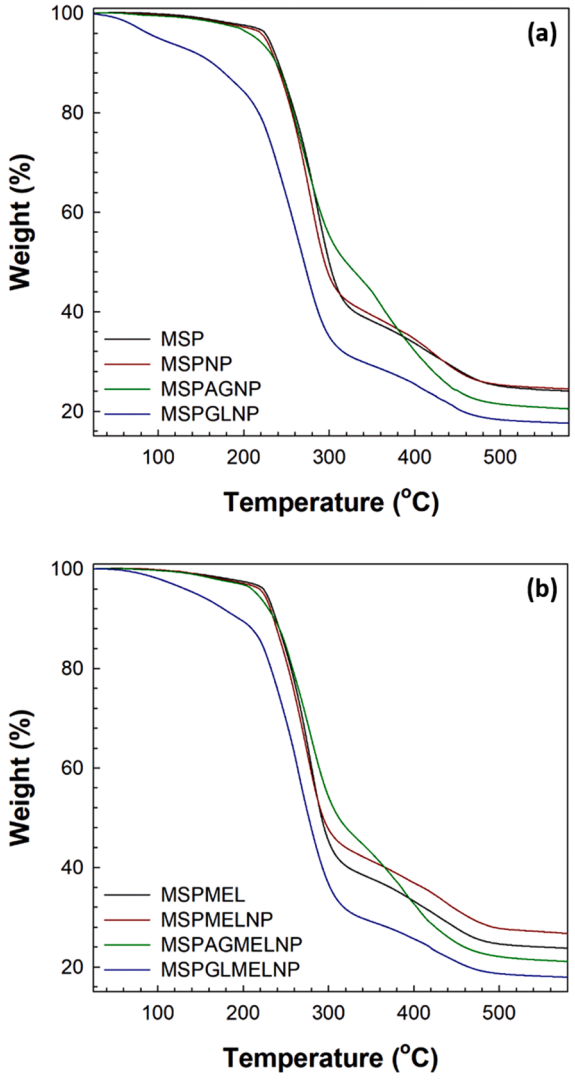

Fig. 6. TGA of the prepared biomaterials. (a) TGA curves of the functional biomaterials without the addition of MEL. (b) TGA curves of the MEL-added functional biomaterials.

3.7. NP release properties using an artificial skin test

To verify the applicability of the functional NP-incorporated biomaterials for treating inflammation as TDDS, NP release properties were investigated at pH 5.5, 36.5 °C, and RH 60% using artificial skin.

NP release profiles of the NP-incorporated biomaterials without NIR laser irradiation and with/without MEL and plasticizers (AG and GL) using an artificial skin are shown in Fig. 8. Results indicated that cumulative concentrations of NP release for the prepared NP-incorporated biomaterials were increased at a relatively steady rate for 180 min. In addition, the NP release ratios (%) of biomaterials with/without the addition of MEL were almost identical during release times. However, the difference in NP release degrees was revealed depending on the type of plasticizers in the following increasing order: NP-incorporated biomaterial with GL > NP-incorporated biomaterial with AG > NP-incorporated biomaterial without plasticizers. The results could be attributed to the water resistance properties of the prepared biomaterials with plasticizers in DW. The results of water resistance properties such as SB and S revealed that the water resistance properties of the prepared biomaterials with AG and GL were relatively lower than those of the biomaterials without plasticizers because AG and GL have high solubility in DW (see Fig. 1b). Therefore, the relatively high NA release of NA-incorporated biomaterials can be attributed to the flexibility and decomposition of biomaterial chains by DW in the prepared complex biomaterials. The simulated results by the Fickian diffusion and empirical model are shown in Table 4. The results of the calculated D_e values using the Fickian diffusion model indicated that the NP release rate was in the following order: MSPGLMELNP (1.464E-11) > MSPGLNP (1.456E-11) > MSPAGMELNP (1.387E-11) > MSPAGNP (1.379E-11) > MSPMELNP (1.330E-11) > MSPMELNP (1.324E-11). The results revealed that there was no significant difference between the MEL and NP release rates as a result of the addition of plasticizers (AG and GL). In addition, these results of NP release using artificial skin indicated that the NP release evaluated using the empirical model was more suitable than that with the Fickian diffusion model. Furthermore, because the n

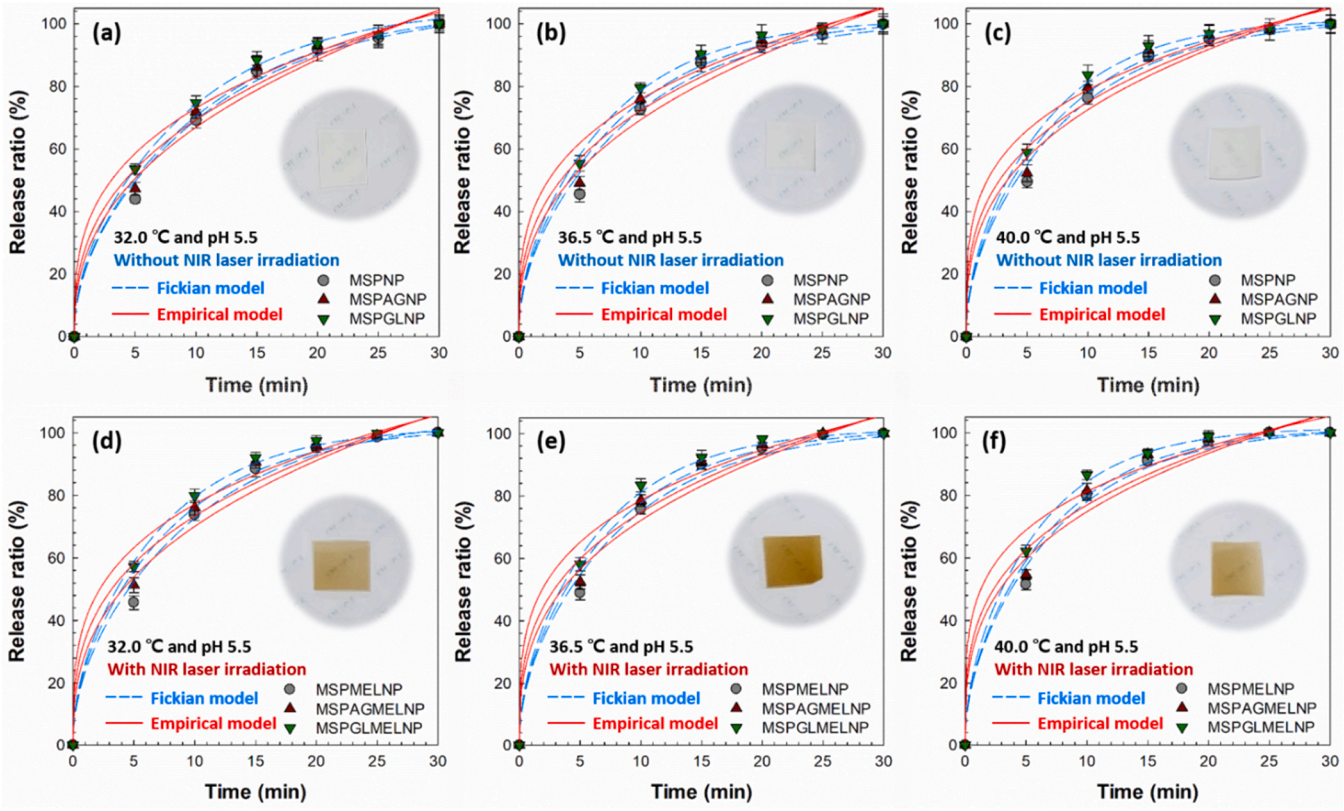

Fig. 7. NP release properties of NP-incorporated biomaterials at various temperatures and pH 5.5 buffer solution. (a-c) NP release (%) from NP-incorporated biomaterials without the addition of MEL and NIR laser irradiation. (d-f) NP release (%) from MEL-added NP-incorporated biomaterials using NIR laser irradiation. The symbols represent experimental data and the long dash line (Fickian) and solid line (empirical) depict model prediction.

Table 3
Fickian diffusion and empirical model parameters of NP release from NP-incorporated biomaterials and from MEL-added NP-incorporated biomaterials with NIR laser irradiation at various temperatures and pH 5.5.

Fickian diffusion model									
	MSPNP			MSPAGNP			MSPGLNP		
T(℃)	32.0	36.5	40.0	32.0	36.5	40.0	32.0	36.5	40.0
Q_∞	105.670	101.743	101.764	105.758	101.761	101.773	105.853	101.764	101.785
D_e	1.248 E-10	1.502 E-10	1.664 E-10	1.297 E-10	1.646 E-10	1.813 E-10	1.458 E-10	1.852 E-10	2.036 E-10
R^2	0.993	0.990	0.993	0.995	0.992	0.994	0.997	0.997	0.997
Empirical model									
	MSPNP			MSPAGNP			MSPGLNP		
T(℃)	32.0	36.5	40.0	32.0	36.5	40.0	32.0	36.5	40.0
Q_∞	131.036	137.325	147.394	138.925	145.834	155.070	186.963	194.505	206.637
k	0.201	0.211	0.224	0.211	0.224	0.236	0.188	0.198	0.210
n	0.405	0.379	0.341	0.373	0.345	0.312	0.319	0.295	0.259
R^2	0.841	0.833	0.857	0.854	0.866	0.861	0.859	0.853	0.839
Fickian diffusion model									
	MSPMELNP			MSPAGMELNP			MSPGLMELNP		
T(℃)	32.0	36.5	40.0	32.0	36.5	40.0	32.0	36.5	40.0
Q_∞	105.867	101.772	101.784	102.081	101.780	101.791	102.130	101.788	101.814
D_e	1.486 E-10	1.644 E-10	1.811 E-10	1.694 E-10	1.801 E-10	1.926 E-10	1.891 E-10	2.021 E-10	2.164 E-10
R^2	0.991	0.991	0.992	0.994	0.994	0.994	0.997	0.997	0.994
Empirical model									
	MSPMELNP			MSPAGMELNP			MSPGLMELNP		
T(℃)	32.0	36.5	40.0	32.0	36.5	40.0	32.0	36.5	40.0
Q_∞	120.921	127.671	136.988	148.803	149.457	152.518	150.843	152.410	157.329
k	0.172	0.181	0.371	0.229	0.240	0.277	0.286	0.269	0.234
n	0.378	0.351	0.236	0.333	0.319	0.296	0.253	0.281	0.322
R^2	0.839	0.853	0.824	0.852	0.831	0.847	0.835	0.828	0.826

values of the empirical model parameter were greater than 0.5 for the prepared NP-incorporated biomaterials regardless of the addition of plasticizer, the NP release properties using artificial skin followed a non-Fickian diffusion mechanism.

Fig. 9 shows the results of comparing the NP release behavior with NIR laser irradiation for 30 min of the prepared NP-incorporated biomaterials with/without the addition of MEL. In the case of the prepared NP-incorporated biomaterials without MEL, the NP release ratio (%)

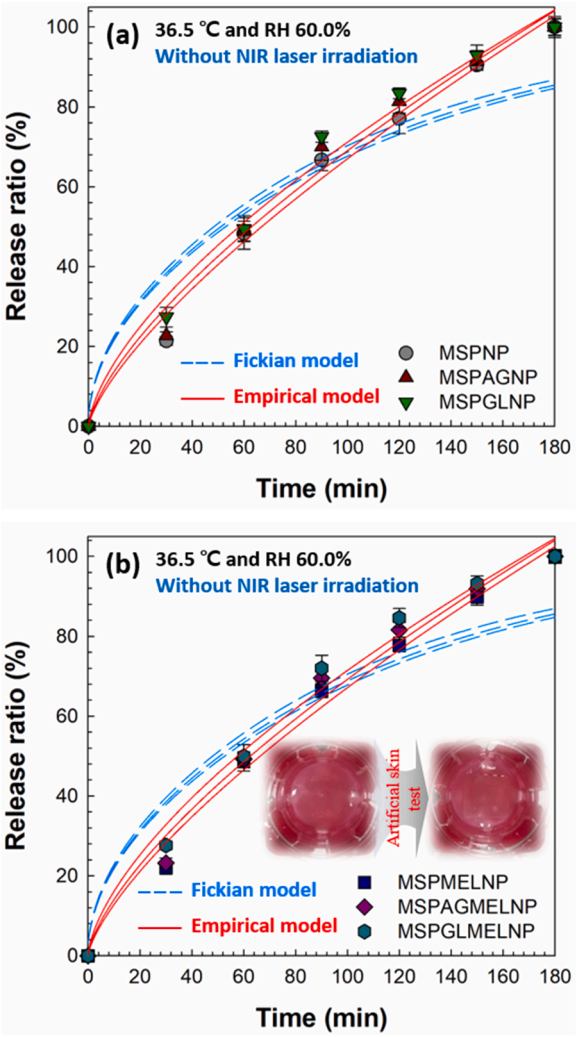

Fig. 8. NP release properties of NP-incorporated biomaterials without NIR laser irradiation using artificial skin. (a) NP release ratio (%) from NP-incorporated biomaterials without the addition of MEL. (b) MEL-added NP release (%) from NP-incorporated biomaterials.

gradually increased for 30 min to about 22.0 – 32.2% (see Fig. 9a). Fig. 9b presents the results of the NP release ratio (%) from MEL-added NP-incorporated biomaterials with NIR laser irradiation for 30 min. When compared to the biomaterials without NIR laser irradiation, there was no significant difference in NP release. However, when irradiated with a NIR laser, the NP release ratio (%) of biomaterials with MEL rapidly increased to 93.1 – 94.5% for 30 min. In addition, the NP release ratio (%) of the NP-incorporated biomaterials with MEL was about 3.0 – 3.2 times higher than that without the addition of MEL. These results were attributed to the effective penetration of NP into artificial skin owing to the heat generated by the photothermal effect of MEL. Fig. 9c shows the NP release properties from MEL-added NP-incorporated biomaterials when NIR laser was irradiated using an on/off running at 5-minute intervals for 30 min. Results indicated that NP release was increased step by step by on/off running of NIR laser irradiation. In addition, it could be confirmed that NP release increased about 2.0–2.5 times when NIR laser was irradiated. Table 5 presents the calculated results using the Fickian diffusion and empirical model. These results revealed that the NP release properties with NIR laser irradiation using the empirical model were more satisfactory than those using the Fickian diffusion model. In addition, the n values of the NP-incorporated biomaterials with NIR laser simulated by the empirical model were greater than 0.5, confirming that the NP release properties with NIR laser using artificial skin followed a non-Fickian diffusion mechanism. These results indicated that the functional NP-incorporated biomaterials had the potential for TDDS and confirmed that they could be used to treat acute inflammation with controlled drug release using the photothermal effect.

4. Conclusions

Functional naproxen (NP)-incorporated biomaterials comprising MS, PVA, MEL, and plasticizers (AG and GL) were successfully prepared using the casting method and UV curing process. From the investigation of SB and S in DW, it was found that the optimal UV curing time for the preparation of the NP-incorporated biomaterials was 30 min. In addition, the chemical structure, surface morphology, and cross-section morphology of the prepared biomaterials were characterized by FT-IR, FE-SEM and TGA analysis. The evaluation of photothermal conversion efficiencies of the prepared biomaterials with/without MEL was conducted under 808 NIR laser irradiation at 1.5 W/cm^2. The results confirmed that the change in temperature of the biomaterials with MEL was about 1.35 – 1.46 times higher than those of biomaterials without the addition of MEL. To apply TDDS for treating inflammation, the NP release properties were evaluated at various temperatures at pH 5.5. Results indicated that the NP release ratio (%) increased with increasing temperature. In addition, the results of applying a mathematical model of NP release behavior demonstrated that the Fickian diffusion model was more suitable than the empirical model. The NP release profiles using artificial skin indicated that the degree of NP release increased consistently for 3 h in the NP-incorporated biomaterials with/without the addition of MEL when NIR laser was not irradiated. However, when irradiated with NIR laser, the NP release ratio (%) of biomaterials with MEL rapidly increased to 93.1 – 94.5% for 30 min. In addition, the NP release of biomaterials with MEL was about 3.0 – 3.2 times higher than that of the biomaterials without MEL. The NP release mechanisms using artificial skin could be explained by the empirical model because NP

Table 4
Fickian diffusion and empirical model parameters of NP release from NP-incorporated biomaterials using various pH of artificial skin at 36.5 ℃ and RH 60%.

Fickian diffusion model									
	MSPNP			MSPAGNP			MSPGLNP		
pH	4.5	5.5	6.5	4.5	5.5	6.5	4.5	5.5	6.5
Q_∞	100.567	100.551	100.524	100.258	100,259	100.292	100.260	100.258	100.254
D_e	1.412 E-11	1.324 E-11	1.172 E-11	1.429 E-11	1.379 E-11	1.326 E-11	1.522 E-11	1.456 E-11	1.380 E-11
R^2	0.873	0.866	0.837	0.874	0.864	0.855	0.887	0.879	0.861
Empirical model									
	MSPNP			MSPAGNP			MSPGLNP		
pH	4.5	5.5	6.5	4.5	5.5	6.5	4.5	5.5	6.5
Q_∞	90.176	81.416	60.306	57.703	52.640	57.663	65.267	59.655	51.690
k	0.0321	0.0289	0.0214	0.0579	0.0528	0.0269	0.0655	0.0599	0.0519
n	0.690	0.727	0.842	0.663	0.698	0.757	0.616	0.650	0.706
R^2	0.989	0.990	0.996	0.986	0.987	0.990	0.987	0.988	0.985

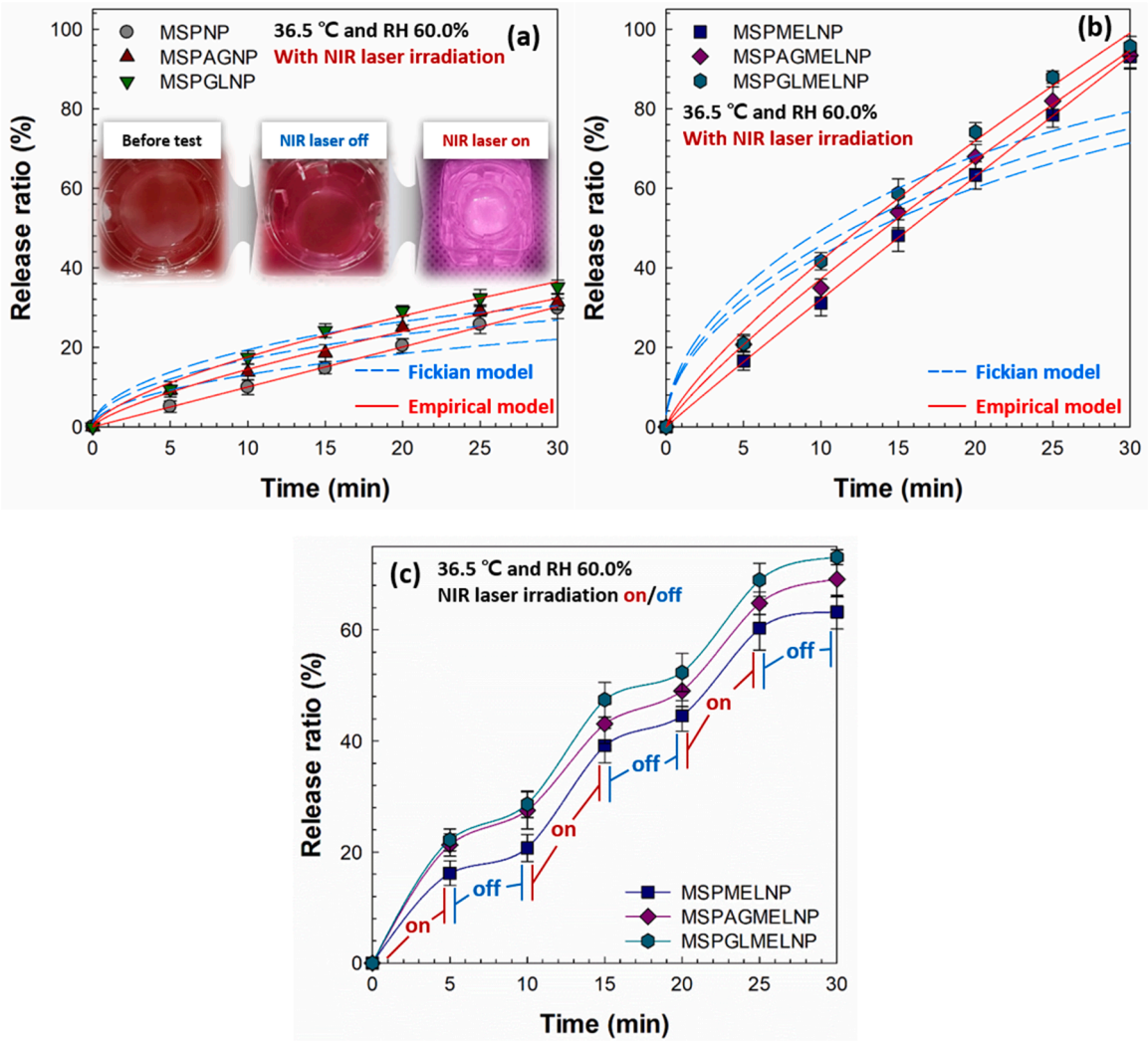

Fig. 9. NP release properties of NP-incorporated biomaterials with NIR laser irradiation using artificial skin. (a) NP release ratio (%) from NP-incorporated biomaterials without the addition of MEL. (b) MEL-added NP release (%) from NP-incorporated biomaterials. (c) MEL-added NP release (%) from NP-incorporated biomaterials with an on/off running of NIR laser irradiation. The symbols represent experimental data and the long dash line (Fickian) and solid line (empirical) depict model prediction.

Table 5
Fickian diffusion and empirical model parameters of NP release from functional NP-incorporated biomaterials with NIR laser irradiation using artificial skin at pH 5.5, 36.5 ℃ and RH 60%.

Fickian diffusion model				
	MSPNP	MSPMELNP	MSPAGMELNP	MSPGLMELNP
Q_∞	30.246	93.508	96.1526	95.565
D_e	5.306E-11	5.9872E-11	6.346E-11	7.569E-11
R^2	0.827	0.853	0.888	0.898
Empirical model				
	MSPNP	MSPMELNP	MSPAGMELNP	MSPGLMELNP
Q_∞	24.776	117.354	100.442	134.2259
k	0.0399	0.0290	0.0522	0.0508
n	1.005	0.974	0.851	0.787
R^2	0.999	0.999	0.998	0.996

release behavior followed a non-Fickian diffusion mechanism. Thus, these results confirmed the applicability of the controlled drug release of NP-incorporated biomaterials with MEL in treating acute inflammation.

Declaration of Competing Interest

The authors declare that they have no known competing financial interests or personal relationships that could have appeared to influence the work reported in this paper.

Data Availability

Data will be made available on request.

Acknowledgment

This research was supported by Basic Science Research Program through the National Research Foundation of Korea (NRF) funded by the Ministry of Education (Grant no. NRF-2019R1I1A3A01061508).

References

[1] I. Pashkuleva, A.P. Marques, F. Vaz, R.L. Reis, Surface modification of starch based biomaterials by oxygen plasma or UV-irradiation, J. Mater. Sci. Mater. Med. 21 (2010) 21–32.
[2] Y. Zhong, P. Godwin, Y. Jin, H. Xiao, Biodegradable polymers and green-based antimicrobial packaging materials: A mini-review, Adv. Ind. Eng. Polym. Res. 3 (2020) 27–35.

[3] Y. Zhang, L. Dong, L. Liu, Z. Wu, D. Pan, L. Liu, Recent advances of stimuli-responsive polysaccharide hydrogels in delivery systems: A review, J. Agric. Food Chem. 70 (2022) 6300–6316.
[4] Y. Zhu, C. Romain, C.K. Williams, Sustainable polymers from renewable resources, Nature 540 (2016) 354–362.
[5] V. Sessini, M.P. Arrieta, A. Fernández-Torres, L. Peponi, Humidity-activated shape memory effect on plasticized starch-based biomaterials, Carbohydr. Polym. 179 (2018) 93–99.
[6] F.G. Torres, S. Commeaux, O.P. Troncoso, Starch-based biomaterials for wound-dressing applications, Stärke 65 (2013) 543–551.
[7] X.L. Wang, K.K. Yang, Y.Z. Wang, Properties of starch blends with biodegradable polymers, J. Macromol. Sci. Polym. Rev. 43 (2003) 385–409.
[8] M.H. Aboumanei, A.F. Mahmoud, Design and development of a proniosomal transdermal drug delivery system of caffeine for management of migraine: In vitro characterization, 131I-radiolabeling and in vivo biodistribution studies, Process. Biochem. 97 (2020) 201–212.
[9] M.R. Prausnitz, S. Mitragotri, R. Langer, Current status and future potential of transdermal drug delivery, Nat. Rev. Drug Discov. 3 (2004) 115–124.
[10] R. Hoover, Y.X. Li, G. Hynes, N. Senanayake, Physicochemical characterization of mung bean starch, Food Hydrocoll. 11 (1997) 401–408.
[11] H.Y. Tak, Y.H. Yun, C.M. Lee, S.D. Yoon, Sulindac imprinted mungbean starch/PVA biomaterial films as a transdermal drug delivery patch, Carbohydr. Polym. 208 (2019) 261–268.
[12] H.S. Kim, Y.H. Yun, W.G. Shim, S.D. Yoon, Preparation of atenolol imprinted polysaccharide based biomaterials for a transdermal drug delivery system, J. Drug Deliv. Sci. Technol. 59 (2020), 101893.
[13] H.S. Kim, Y.H. Yun, W.G. Shim, S.D. Yoon, Preparation and evaluation of functional allopurinol imprinted starch based biomaterials for transdermal drug delivery, Int. J. Biol. Macromol. 175 (2021) 217–228.
[14] S.Y. Park, J.H. Kang, H.S. Kim, J.Y. Hwang, U.S. Shin, Electrical and thermal stimulus-responsive nanocarbon-based 3D hydrogel sponge for switchable drug delivery, Nanoscale 14 (2022) 2367–2382.
[15] R. Teodorescu, G. Quéniat, C. Foulon, M. Lecoeur, A. Barras, S. Boulahneche, M. S. Medjram, T. Hubert, A. Abderrahmani, R. Boukherroub, S. Szunerits, Transdermal skin patch based on reduced graphene oxide: A new approach for photothermal triggered permeation of ondansetron across porcine skin, J. Control. Release 245 (2017) 137–146.
[16] Y. Qiu, K. Park, Environment-sensitive hydrogels for drug delivery, Adv. Drug Deliv. Rev. 53 (2001) 321–339.
[17] D. Huang, M. Sun, Y. Bu, F. Luo, C. Lin, Z. Lin, Z. Weng, F. Yang, D. Wu, Microcapsule-embedded hydrogel patches for ultrasound responsive and enhanced transdermal delivery of diclofenac sodium, J. Mater. Chem. B 7 (2019) 2330–2337.
[18] R. Cheng, F. Meng, C. Deng, H.A. Klok, Z. Zhong, Dual and multi-stimuli responsive polymeric nanoparticles for programmed site-specific drug delivery, Biomaterials 34 (2013) 3647–3657.
[19] F. Zhang, G. Lu, X. Wen, F. Li, X. Ji, Q. Li, M. Wu, Q. Cheng, Y. Yu, J. Tang, L. Mei, Magnetic nanoparticles coated with polyphenols for spatio-temporally controlled cancer photothermal/immunotherapy, J. Control. Release 326 (2020) 131–139.
[20] C. Xu, Y. Xu, M. Yang, Y. chang, A. Nie, Z. Liu, J. Wang, Z. Luo, Black-phosphorus-incorporated hydrogel as a conductive and biodegradable platform for enhancement of the neural differentiation of mesenchymal stem cells, Adv. Funct. Mater. 21 (2010) 21–32.
[21] X. Zeng, M. Luo, G. Liu, X. Wang, W. Tao, Y. Lin, X. Ji, L. Nie, L. Mei, Polydopamine-modified black phosphorous nanocapsule with enhanced stability and photothermal performance for tumor multimodal treatments, Adv. Sci. 5 (2018) 1800510.
[22] M. Ou, C. Lin, Y. Wang, Y. Lu, W. Wang, Z. Li, W. Zeng, X. Zeng, X. Ji, L. Mei, Heterojunction engineered bioactive chlorella for cascade promoted cancer therapy, J. Control. Release 345 (2022) 755–769.
[23] T. Chen, W. Zeng, C. Tie, M. Yu, H. Hao, Y. Deng, Q. Li, H. Zheng, M. Wu, L. Mei, Engineered gold/black phosphorus nanoplatforms with remodeling tumor microenvironment for sonoactivated catalytic tumor theranostics, Bioact. Mater. 10 (2022) 515–525.
[24] Y. Yue, X. Zhao, Melanin-like nanomedicine in photothermal therapy applications, Int. J. Mol. Sci. 22 (2021) 399.
[25] Y. Li, X. Liu, W. Pan, N. Li, B. Tang, Photothermal therapy-induced immunogenic cell death based on natural melanin nanoparticles against breast cancer, Chem. Commun. 56 (2020) 1389–1392.
[26] Y. Liu, K. Ai, J. Liu, M. Deng, Y. He, L. Lu, Dopamine-melanin colloidal nanospheres: an efficient near-infrared photothermal therapeutic agent for in vivo cancer therapy, Adv. Mater. 25 (2013) 1353–1359.
[27] K.K. Petersen, M.L. Rousing, C. Jensen, L. Arendt-Nielsen, P. Gazerani, Effect of local controlled heat on transdermal delivery of nicotine, Int. J. Physiol. Pathophysiol. Pharmacol. 3 (2011) 236–242.
[28] I. Vanakoski, T. Seppälä, Heat exposure and drugs, Clin. Pharmacokinet. 34 (1998) 311–322.
[29] C. Nathan, Points of control in inflammation, Nature 420 (2002) 846–852.
[30] D. Furman, J. Campisi, E. Verdin, P.C. Bastos, S. Targ, C. Franceschi, L. Ferricci, D. W. Gilroy, A. Fasano, G.W. Miller, A.H. Miller, A. Mantovani, C.M. Weyand, N. Barzilai, J.J. Goronzy, T.A. Rando, R.B. Effros, A. Lucia, N. Kleinstreuer, G. M. Slavich, Chronic inflammation in the etiology of disease across the life span, Nat. Med. 25 (2019) 1822–1832.
[31] F.R. Greten, S.I. Grivennikov, Inflammation and cancer: triggers, mechanisms, and consequences, Immunity 51 (2019) 27–41.
[32] E. Ricciotti, G.A. Fitzgerald, Prostaglandins and inflammation, Arter. Throm. Vas. 31 (2011) 986–1000.
[33] B.D. Levy, C.N. Serhan, Resolution of acute inflammation in the lung, Annu. Rev. Physiol. 76 (2014) 467–492.
[34] S. Patnaik, A.D. Kurdekar, L.A. Chunduri, C. Prathibha, K. Venktaramaniah, In vitro dissolution studies on naproxen-PVP nanoformulations show enhanced oral bioavailability of naproxen, Int. J. Med. Nano Res. 5 (2018) 023.
[35] R.P. Bhole, S.S. Shinde, S.S. Chitlange, S.B. Wankhede, A high-performance thin layer chromatography (HPTLC) method for simultaneous determination of diphenhydramine hydrochloride and naproxen sodium in tablets, Anal. Chem. Insights 10 (2015) 47–51.
[36] A.L. Biobaum, S. Xu, S.W. Rowlinson, K.C. Duggan, S. Banerjee, S.N. Kudalkar, W. R. Birmingham, K. Ghebreselasie, L.J. Marnett, Action at a distance: mutations of peripheral residues transform rapid reversible inhibitors to slow, tight binders of cyclooxygenase-2, J. Biol. Chem. 290 (2015) 12793–12803.
[37] K. Brune, Persistence of NSAIDs at effect sites and rapid disappearance from side-effect compartments contributes to tolerability, Curr. Med. Res. Opin. 23 (2007) 2985–2995.
[38] K.H. Maniar, I.A. Jones, R. Gopalakrishna, C.T. Vangsness Jr, Lowering side effects of NSAID usage in osteoarthritis: recent attempts at minimizing dosage, Expert Opin. Pharmacol. 19 (2018) 93–102.
[39] H.S. Kim, C.M. Lee, Y.H. Yun, Y.S. Kim, S.D. Yoon, Synthesis and drug release properties of melanin added functional allopurinol incorporated starch-based biomaterials, Int. J. Biol. Macromol. 209 (2022) 1477–1485.
[40] E. Proksch, pH in nature, humans and skin, J. Dermatol. 45 (2018) 1044–1052.
[41] K.M. Hanson, M.J. Behne, N.P. Barry, T.M. Mauro, E. Gratton, R.M. Clegg, Two-photon fluorescence lifetime imaging of the skin stratum corneum pH gradient, Biophys. J. 83 (2002) 1682–1690.
[42] J.F. Rubilar, R.M. Cruz, R.N. Zuñiga, I. Khmelinskii, M.C. Vieira, Mathematical modeling of gallic acid release from chitosan films with grape seed extract and carvacrol, Int. J. Biol. Macromol. 104 (2017) 197–203.
[43] P.L. Ritger, N.A. Peppas, A simple equation for description of solute release I. Fickian and non-fickian release from non-swellable devices in the form of slabs, spheres, cylinders or discs, J. Control. Release 5 (1987) 23–36.
[44] J. Siepmann, N.A. Peppas, Higuchi equation: Derivation, application, use and misuse, Int. J. Pharm. 418 (2011) 6–12.
[45] E.M. Davis, M. Minelli, M.G. Baschetti, Y.A. Elabd, Non-fickian diffusion of water in polylactide, Ind. Eng. Chem. Res. 52 (2013) 8664–8673.
[46] Z. Gu, B. Chen, Y. Tian, Highly branched corn starch: Preparation, encapsulation, and release of ascorbic acid, Food Chem. 343 (2021), 128485.
[47] P.I. Lee, Kinetics of drug release from hydrogel matrices, J. Control. Release 2 (1985) 277–288.
[48] J. Siepmann, N.A. Peppas, Modeling of drug release from delivery systems based on hydroxypropyl methylcellulose (HPMC), Adv. Drug Deliv. Rev. 64 (2012) 163–174.
[49] N.N. Li, C.P. Fu, L.M. Zhan, Using casein and oxidized hyaluronic acid to form biocompatible composite hydrogels for controlled drug release, Mater. Sci. Eng. C 36 (2014) 287–293.
[50] M. Jamrógiewicz, K. Milewska, B. Mikolaszek, Spectroscopic evaluation on pseudopolymorphs of sodium naproxen, Spectrochim. Acta A Mol. Biomol. Spectrosc. 261 (2021), 120018.
[51] S. Javanbakht, N. Nazari, R. Rakhshaei, H. Namazi, Cu-crosslinked carboxymethylcellulose/naproxen/graphene quantum dot nanocomposite hydrogel beads for naproxen oral delivery, Carbohydr. Polym. 195 (2018) 453–459.
[52] G.S. Kiran, S.A. Jackson, S. Priyadharsini, A.D.W. Dobson, J. Selvin, Synthesis of Nm-PHB (nanomelanin-polyhydroxy butyrate) nanocomposite film and its protective effect against biofilm-forming multi drug resistant Staphylococcus aureus, Sci. Rep. 7 (2017) 1–13.
[53] J. Stainsack, A.S. Mangrich, C.M.B.F. Maia, V.G. Machado, J.C.P.D.S. Nakagaki, Spectroscopic investigation of hard and soft metal binding sites in synthetic melanin, Inorg. Chim. Acta 356 (2003) 243–248.
[54] W. Ning, Y. Jiugao, M. Xiaofei, W. Ying, The influence of citric acid on the properties of thermoplastic starch/linear low-density polyethylene blends, Carbohydr. Polym. 67 (2007) 446–453.
[55] B. Xiao, Y. Wan, M. Zhao, Y. Liu, S. Zhang, Preparation and characterization of antimicrobial chitosan-N-arginine with different degrees of substitution, Carbohydr. Polym. 83 (2011) 144–150.
[56] S. Wen, X. Miao, G.C. Fan, T. Xu, L.P. Jiang, P. Wu, C. Cai, J.J. Zhu, Aptamer-conjugated Au nanocage/SiO_2 core-shell bifunctional nanoprobes with high stability and biocompatibility for cellular SERS imaging and Near-Infrared photothermal therapy, ACS Sens 4 (2019) 301–308.
[57] P. Yang, S. Zhang, N. Zhang, Y. Wang, J. Zhong, X. Sun, Y. Qi, X. Chen, Z. Li, Y. Li, Tailoring synthetic melanin nanoparticles for enhanced photothermal therapy, ACS Appl. Mater. Interfaces 11 (2019) 42671–42679.
[58] M.D. Nieuwenhoff, Y. Wu, F.J.P.M. Huygen, A.C. Schouten, F.C.T. van der helm, S. P. Niehof, Reproducibility of axon reflex-related vasodilation assessed by dynamic thermal imaging in healthy subjects, Microvasc. Res. 106 (2016) 1–7.
[59] P. Gazerani, L.A. Nielsen, Cutaneous vasomotor reactions in response to controlled heat applied on various body regions of healthy humans: evaluation of time course and application parameters, Int. J. Physiol. Pathophysiol. Pharmacol. 3 (2011) 202–209.

[60] M. Wei, S. Shi, J. Wang, Y. Li, X. Duan, Studies on the intercalation of naproxen into layered double hydroxide and its thermal decomposition by in situ FT-IR and in situ HT-XRD, J. Solid. State Chem. 177 (2004) 2534–2541.

[61] W. Dong, Y. Wang, C. Huang, S. Xiang, P. Ma, Z. Ni, M. Chen, Enhanced thermal stability of poly (vinyl alcohol) in presence of melanin, J. Therm. Anal. Calor. 115 (2014) 1661–1668.

[62] S.D. Yoon, Cross-linked potato starch-based blend films using ascorbic acid as a plasticizer, J. Agric. Food Chem. 62 (2014) 1755–1764.